PIM1 kinase inhibition as a targeted therapy against triple-negative breast tumors with elevated MYC expression

Dai Horiuchi[1–4], Roman Camarda[1], Alicia Y Zhou[1,11], Christina Yau[5,6], Olga Momcilovic[1], Sanjeev Balakrishnan[1,11], Alexandra N Corella[1,11], Henok Eyob[1,11], Kai Kessenbrock[7,11], Devon A Lawson[7,11], Lindsey A Marsh[3,4], Brittany N Anderton[1,11], Julia Rohrberg[1], Ratika Kunder[3,4], Alexey V Bazarov[8,11], Paul Yaswen[8], Michael T McManus[9], Hope S Rugo[10], Zena Werb[2,7] & Andrei Goga[1,2,10]

Triple-negative breast cancer (TNBC), in which cells lack expression of the estrogen receptor (ER), the progesterone receptor (PR) and the ERBB2 (also known as HER2) receptor, is the breast cancer subtype with the poorest outcome[1]. No targeted therapy is available against this subtype of cancer owing to a lack of validated molecular targets. We previously reported that signaling involving MYC—an essential, pleiotropic transcription factor that regulates the expression of hundreds of genes—is disproportionally higher in triple-negative (TN) tumors than in receptor-positive (RP) tumors[2]. Direct inhibition of the oncogenic transcriptional activity of MYC has been challenging to achieve[3]. Here, by conducting a shRNA screen targeting the kinome, we identified PIM1, a non-essential serine–threonine kinase, in a synthetic lethal interaction with MYC. PIM1 expression was higher in TN tumors than in RP tumors and was associated with poor prognosis in patients with hormone- and HER2-negative tumors. Small-molecule PIM kinase inhibitors halted the growth of human TN tumors with elevated MYC expression in patient-derived tumor xenograft (PDX) and MYC-driven transgenic mouse models of breast cancer by inhibiting the oncogenic transcriptional activity of MYC and restoring the function of the endogenous cell cycle inhibitor, p27. Our findings warrant clinical evaluation of PIM kinase inhibitors in patients with TN tumors that have elevated MYC expression.

Although de-regulated MYC signaling has been identified in a variety of human malignancies, no targeted therapy has been clinically established to treat solid tumors with elevated MYC expression. To date, small molecules designed to directly inhibit MYC transcriptional activity have not been successful in preclinical animal studies[3]. An alternative approach is indirect inhibition of oncogenic MYC activity by the targeting of druggable proteins that are essential for the viability of MYC-driven tumors but not nontumorigenic cells. This indirect treatment strategy has become known as a synthetic lethal approach[4].

To identify new, readily druggable targets for the treatment of MYC-overexpressing TNBCs, we conducted a kinome-wide MYC synthetic lethal shRNA screen in non-immortalized human mammary epithelial cells[5] (HMECs) expressing a 4-hydroxytamoxifen (TAM)-activated *MYC-Esr1* transgene[6] (hereafter referred to as HMEC-*MYC-ER* cells) (**Fig. 1a**). MYC-dependent synthetic lethal screens using mammary epithelial cell systems have been previously reported[7,8]; however, to our knowledge, our screen is the first to use early-passage non-immortalized HMECs (obtained through breast reduction mammoplasty) that lack detectable genomic alterations[9]. This approach allows us to study the response of mammary epithelial cells to oncogenic MYC activation in a highly specific manner, independently of any potential confounding effects of *in vitro* cellular immortalization. Of 600 human kinases targeted by 2,000 individual shRNA clones, we identified nine kinases that were selectively required for the survival of HMEC-*MYC-ER* cells (**Fig. 1a** and **Supplementary Table 1**). Kinase components of the NF-κB, mitogen (ERK and JNK), PI3K–AKT and WNT signaling pathways were identified, most of which had not been identified in prior synthetic lethal screens. Although any of these kinases could potentially serve as a druggable target for the treatment of MYC-overexpressing breast cancer, we decided to pursue further study of PIM1 kinase. Knockdown of *PIM1* expression had the greatest efficacy among the kinase hits in causing cell death

a Reduction mammoplasty → Isogenic, non-immortalized HMEC-*MYC-ER* cells → shRNA lentiviral infection 20 h → −TAM / +TAM (MYC activation) 48 h → Cell viability assay → MYC synthetic lethal partners

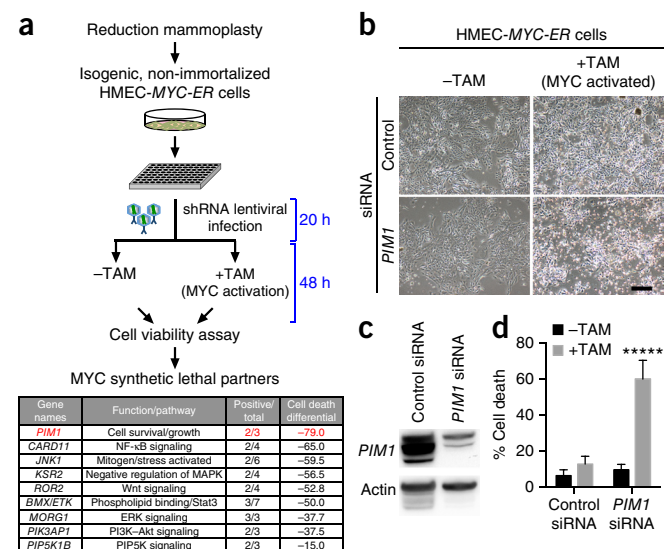| Gene names	Function/pathway	Positive/ total	Cell death differential
PIM1	Cell survival/growth	2/3	−79.0
CARD11	NF-κB signaling	2/4	−65.0
JNK1	Mitogen/stress activated	2/6	−59.5
KSR2	Negative regulation of MAPK	2/4	−56.5
ROR2	Wnt signaling	2/4	−52.8
BMX/ETK	Phospholipid binding/Stat3	3/7	−50.0
MORG1	ERK signaling	3/3	−37.7
PIK3AP1	PI3K–Akt signaling	2/3	−37.5
PIP5K1B	PIP5K signaling	2/3	−15.0

Figure 1 Loss of PIM1 induces synthetic lethality with MYC activation in a model human mammary epithelial cell system. (**a**) Top, schematic representation of the synthetic lethal shRNA screen conducted in this study. HMECs expressing a 4-hydroxytamoxifen (TAM)-activatable *MYC-ER* transgene were infected with a library of viruses expressing shRNAs directed against transcripts encoding the human kinome, using a 96-well format (i.e., one shRNA clone per well), and then treated without or with TAM to induce MYC activation. Bottom, list of genes from the shRNA screen that are synthetic lethal with MYC expression, defined as genes targeted by at least two independent shRNA clones that selectively induced cell death in MYC-activated (+TAM) HMECs. Positive/total refers to the number of shRNA clones that induced MYC-dependent cell death per the total number of shRNA clones in the shRNA library targeting that gene. Cell death differential was calculated as 'percentage growth – percentage death' from averaged values in **Supplementary Table 1**. (**b**) Representative micrographs of HMEC-*MYC-ER* cells after treatment with a control or *PIM1*-specific siRNA, in the absence of presence of TAM ($n = 3$ for each experimental group). Scale bar, 100 μm. (**c**) Representative western blot analysis for PIM1 expression in MYC-activated HMECs that were treated with a *PIM1*-specific ($n = 3$) or control siRNA ($n = 3$). Actin was used as a loading control. (**d**) Viability assay for HMEC-*MYC-ER* cells that were treated ± TAM and with either a *PIM1*-specific or control siRNA, as determined by flow cytometry. The assay was independently repeated five times in triplicate. Error bars represent means ± s.e.m. *****$P < 0.00001$ as determined by a two-tailed *t*-test.

in MYC-activated cells, whereas it had minimal inhibitory effects on the growth of control cells (**Fig. 1a** and **Supplementary Table 1**). The dependence of MYC-activated HMECs on *PIM1* expression for survival was confirmed by treatment of the cells with a pool of four *PIM1*-specific siRNAs (**Fig. 1b–d**), which resulted in a substantial amount of cell death in a MYC-dependent manner.

PIM1 belongs to the PIM family of serine–threonine kinases, which consists of three proto-oncoproteins, PIM1, PIM2 and PIM3 (ref. 10). Knockout mice lacking all three PIM kinases are fully viable and show only minor growth defects, which result in smaller body size[11]. This mild phenotype has raised the hope that PIM kinase inhibitors would induce less systemic toxicity than inhibitors of essential kinases. PIM kinases are thought to have weak tumorigenic capacity on their own[12]. However, PIM1 substantially enhances MYC-induced tumorigenesis in transgenic mouse models of lymphoma and prostate cancer[12,13]. Accordingly, PIM kinase inhibition has been shown to decrease the growth of prostate cancer cells engineered to overexpress *MYC* and *PIM1* (refs. 14,15). However, the efficacy of PIM inhibition as a

MYC-synthetic-lethal therapeutic has not been stringently validated in preclinical animal models, particularly those for breast cancer. Notably, one of the other hits in our screen was *BMX* (also known as *ETK*) (**Fig. 1a** and **Supplementary Table 1**), which encodes a nonreceptor tyrosine kinase that physically interacts with PIM1 (ref. 16), suggesting that multiple components of the PIM1 pathway may have a critical role in MYC-dependent breast tumor growth.

PIM kinase expression and function has been poorly described in human breast cancer. Thus, we first determined receptor-status-specific expression of *PIM1* in primary tumor samples across four distinct publicly available clinical cohorts. In all of the cohorts examined, *PIM1* mRNA expression was significantly elevated in TN tumors as compared to that in hormone receptor (HR)-positive but HER2-negative tumors, and in all but one cohort as compared to *PIM1* mRNA expression in HER2-positive tumors (**Fig. 2a**). Notably, a recent report showed that in the ER-responsive breast cancer cell line MCF7, *PIM1* expression could be induced not only by ER activation with estrogen but also by depletion of estrogen receptor alpha (ERα) when the cells were cultured in the absence of estrogen[17]. Thus, although the precise mechanism by which ER signaling modulates *PIM1* expression remains to be elucidated, loss of expression of HRs, such as ERα, during the process of primary tumor development may contribute to the upregulation of *PIM1* expression that is observed in primary human TN tumors. Consistent with a prior observation that *PIM1* expression is associated with higher-grade breast tumors[17], we found that, for two of the three clinical cohorts that had long-term patient outcome data, increased *PIM1* expression was associated with poor prognosis, as defined by either diminished recurrence-free or distant-metastasis-free survival, in patients with HR-negative tumors (**Fig. 2b,c**).

We also examined receptor-status-specific expression and prognostic value of the other PIM kinase family members, PIM2 and PIM3. We found a tendency for *PIM2* expression to be increased in TN tumors; however, the extent of this increase was not as consistent as that found for PIM1 (**Supplementary Fig. 1a**), and neither was the prognostic value of *PIM2* as consistent as that of PIM1 (**Supplementary Fig. 1b,c**). Our analysis did not find an association of *PIM3* expression with any specific receptor status and did not reveal prognostic value for *PIM3* expression (**Supplementary Fig. 2**).

We next sought to determine whether a MYC-dependent transcriptional gene signature (hereafter referred to as MYC gene signature) and *PIM1* expression are independently associated with survival across several clinical cohorts, using multivariate Cox proportional-hazard modeling (**Fig. 2d**). In the HR-negative subset of the two largest clinical cohorts, increased *PIM1* expression was associated with a significantly higher risk of recurrence, independently of a MYC gene signature. In the I-SPY1 data set, the smallest cohort, a MYC gene signature was significantly associated with worse outcome[2] independently of *PIM1* expression (**Fig. 2d**). Thus, although both *MYC* and *PIM1* are overexpressed in TNBCs (**Fig. 2a** and ref. 2), and overexpression of each of these genes is associated with patient outcome, these associations are independent from one another. These findings indicate that the poor outcome associated with high levels of *PIM1* expression across several data sets is independent of the presence of a MYC gene signature (**Fig. 2d**).

To assess the feasibility of PIM1 inhibition as a therapy for TN tumors with elevated MYC expression, we treated a panel of breast cancer cell lines with a *PIM1*-specific siRNA and studied the effects on cell proliferation and cell death (**Fig. 3a–f**). This panel included a nontumor cell line (HMEC) and ten breast cancer cell lines with varying degrees of MYC and PIM1 expression (**Fig. 3a**). *PIM1*-specific
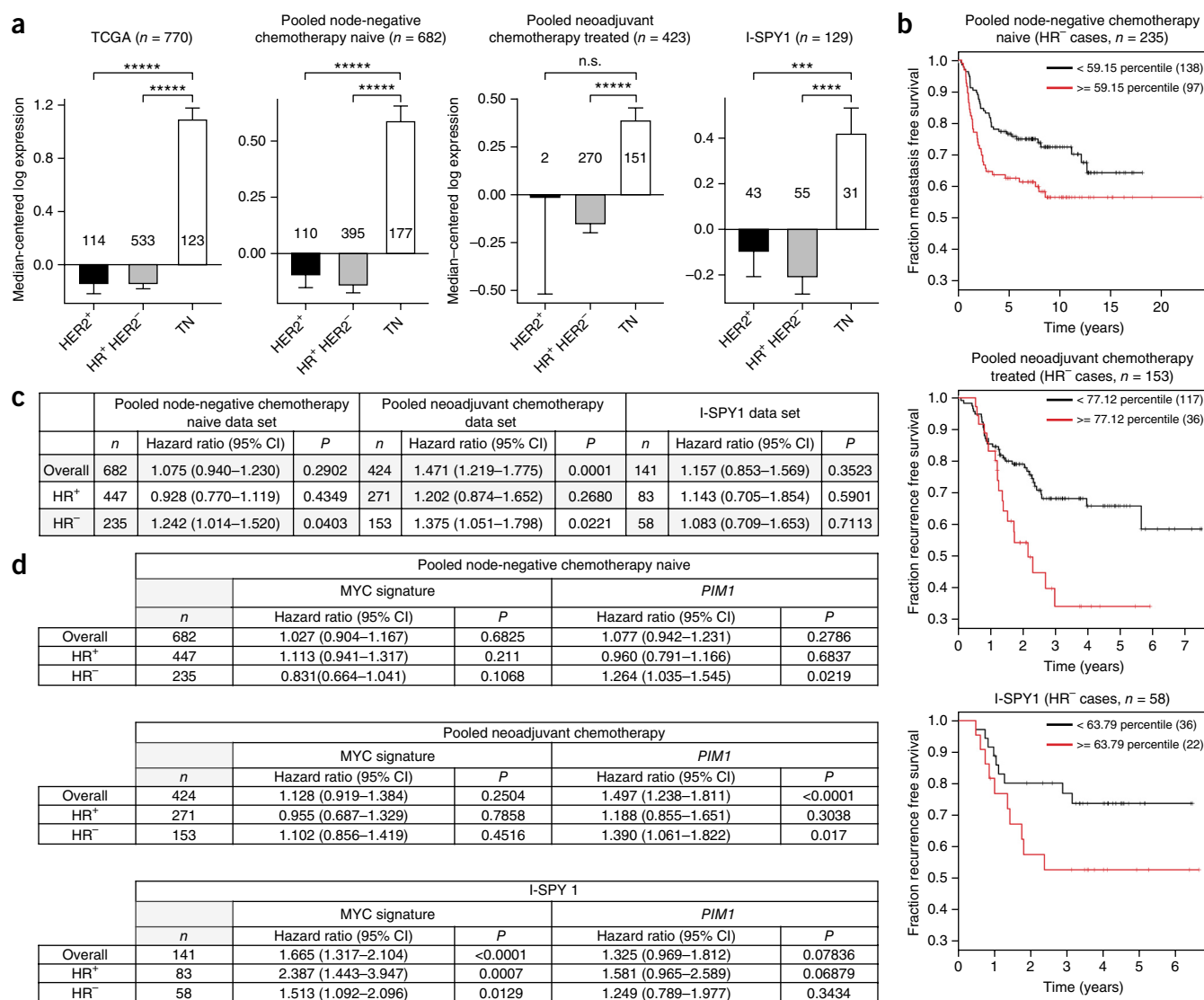
a — *PIM1* mRNA expression in primary breast tumor samples from the TCGA cohort (n = 770), a pooled node-negative chemotherapy naive cohort (n = 682), a pooled neoadjuvant chemotherapy treated cohort (n = 423) and the I-SPY1 cohort (n = 129), stratified by receptor status.

b — Kaplan–Meier graphs: Pooled node-negative chemotherapy naive (HR⁻ cases, n = 235); Pooled neoadjuvant chemotherapy treated (HR⁻ cases, n = 153); I-SPY1 (HR⁻ cases, n = 58).

c

	Pooled node-negative chemotherapy naive data set			Pooled neoadjuvant chemotherapy data set			I-SPY1 data set		
	n	Hazard ratio (95% CI)	P	n	Hazard ratio (95% CI)	P	n	Hazard ratio (95% CI)	P
Overall	682	1.075 (0.940–1.230)	0.2902	424	1.471 (1.219–1.775)	0.0001	141	1.157 (0.853–1.569)	0.3523
HR⁺	447	0.928 (0.770–1.119)	0.4349	271	1.202 (0.874–1.652)	0.2680	83	1.143 (0.705–1.854)	0.5901
HR⁻	235	1.242 (1.014–1.520)	0.0403	153	1.375 (1.051–1.798)	0.0221	58	1.083 (0.709–1.653)	0.7113

d

Pooled node-negative chemotherapy naive					
		MYC signature		*PIM1*	
	n	Hazard ratio (95% CI)	P	Hazard ratio (95% CI)	P
Overall	682	1.027 (0.904–1.167)	0.6825	1.077 (0.942–1.231)	0.2786
HR⁺	447	1.113 (0.941–1.317)	0.211	0.960 (0.791–1.166)	0.6837
HR⁻	235	0.831(0.664–1.041)	0.1068	1.264 (1.035–1.545)	0.0219

Pooled neoadjuvant chemotherapy					
		MYC signature		*PIM1*	
	n	Hazard ratio (95% CI)	P	Hazard ratio (95% CI)	P
Overall	424	1.128 (0.919–1.384)	0.2504	1.497 (1.238–1.811)	<0.0001
HR⁺	271	0.955 (0.687–1.329)	0.7858	1.188 (0.855–1.651)	0.3038
HR⁻	153	1.102 (0.856–1.419)	0.4516	1.390 (1.061–1.822)	0.017

I-SPY 1					
		MYC signature		*PIM1*	
	n	Hazard ratio (95% CI)	P	Hazard ratio (95% CI)	P
Overall	141	1.665 (1.317–2.104)	<0.0001	1.325 (0.969–1.812)	0.07836
HR⁺	83	2.387 (1.443–3.947)	0.0007	1.581 (0.965–2.589)	0.06879
HR⁻	58	1.513 (1.092–2.096)	0.0129	1.249 (0.789–1.977)	0.3434

Figure 2 *PIM1* expression is disproportionally increased in human primary TN tumor samples and is associated with poor clinical outcomes in patients with HR-negative breast cancer. (**a**) *PIM1* mRNA expression in primary breast tumor samples from the TCGA cohort (left), a pooled node-negative chemotherapy-naive cohort (middle left), a pooled neoadjuvant chemotherapy (taxane and anthracycline)-treated cohort (middle right) and the I-SPY1 cohort (right), stratified by receptor status. Values are $\log_2$-transformed and median-centered. Numbers above or within the bars indicate sample size. Error bars represent means ± s.e.m. *****$P < 0.00001$; n.s., not significant; by pairwise two-tailed *t*-tests between the respective groups. (**b**) Kaplan–Meier graphs showing the fraction of patients with metastasis-free survival or recurrence-free survival for the patients with HR-negative tumors, dichotomized by *PIM1* mRNA expression at an optimal threshold, from node-negative chemotherapy-naive (top), pooled neoadjuvant chemotherapy-treated (middle) and I-SPY1 (bottom) cohorts. Samples with increased *PIM1* expression are represented with red lines. Sample size is indicated in parentheses. (**c**) Univariate Cox analysis indicating the association between *PIM1* mRNA expression and survival in pooled node-negative chemotherapy-naive, pooled neoadjuvant chemotherapy (taxane and anthracycline)-treated and I-SPY1 cohorts, specifically in HR-positive and HR-negative subsets. PR status was not available for the pooled node-negative chemotherapy-naive data set; accordingly, ER⁻ and ER⁺ subsets were considered instead. Hazard ratios for a 1 s.d. increase in *PIM1* expression are shown. *P* values were determined by the Wald test. (**d**) Multivariate Cox analysis indicating the association of *PIM1* mRNA expression and MYC gene expression signature with survival in pooled node-negative chemotherapy-naive, pooled neoadjuvant chemotherapy (taxane and anthracycline)-treated and I-SPY1 cohorts, specifically in HR-positive and HR-negative subsets. PR status was not available for the pooled node-negative chemotherapy-naive data set; accordingly, ER⁻ and ER⁺ subsets were considered instead. Hazard ratios for a 1 s.d. increase in *PIM1* expression or MYC signature score are shown. *P* values were determined by the Wald test.

siRNA treatment significantly decreased the proliferation of a number of breast cancer cell lines (**Fig. 3b**,**c**) and also induced appreciable amounts of cell death (**Fig. 3e**). We asked whether a correlation exists between the sensitivity of the cell lines to *PIM1* inhibition and protein levels of MYC and PIM1. As assessed by the relative sensitivity of the cell lines, the levels of MYC protein expression, and that of PIM1 to a lesser extent, significantly correlated with the sensitivity of the cell

lines to *PIM1* knockdown (**Fig. 3d**,**f**). We also observed a correlation between *MYC* mRNA expression and sensitivity to *PIM1* knockdown (**Supplementary Fig. 3**), although this correlation was less significant than that for MYC protein expression.

We noticed that the effect of *PIM1* knockdown was rather short-lived in some of the cell lines (**Fig. 3b** and **Supplementary Fig. 4a**), consistent with prior observations that *PIM1* mRNA and PIM1

protein have short half-lives and that PIM kinases are highly regulated at both the transcriptional and post-translational levels to maintain higher protein expression in tumors[10]. We next asked whether *PIM1* knockdown could influence expression of other PIM kinases, namely PIM2, whose expression was found to be increased in TN tumors in some of the clinical cohorts (**Supplementary Fig. 1a**). *PIM1*-specific siRNA treatment of MDA-MB-231 cells, which show high expression of both MYC and PIM1, resulted in an increase in PIM2 protein expression, whereas *PIM2*-specific siRNA treatment did not seem to activate a similar compensatory response with respect to PIM1 expression (**Supplementary Fig. 4a**). *PIM2*-specific siRNA treatment was as effective as *PIM1*-specific siRNA treatment in inhibiting cell proliferation of MDA-MB-231 cells, and it was more effective in inducing cell death (**Supplementary Fig. 4b,c**). These observations suggest that simultaneous inhibition of multiple PIM kinases may prove particularly efficacious in the treatment of breast tumors with elevated *MYC* and *PIM1* expression.

We next evaluated the effect of PIM kinase inhibition, using the pan–PIM kinase inhibitor SGI-1776 (ref. 18), on the *in vivo* growth of breast cancer cell lines that were injected subcutaneously as xenografts into immunocompromised mice. Tumors derived from the TN line MDA-MB-231 (high levels of MYC and PIM1) and the RP line T47D (low levels of MYC and medium levels of PIM1), which showed differential sensitivity to *PIM1*-specific siRNA in cell culture, were grown until they reached ~200 mm^3 in size. The tumor-bearing mice were then treated with 75 mg per kg body weight (mg/kg) SGI-1776 or vehicle control daily via oral gavage for 14 d. SGI-1776 treatment significantly reduced MDA-MB-231, but not T47D, xenograft tumor growth (**Fig. 3g**).

For a more stringent preclinical assessment of the efficacy of PIM kinase inhibition in treating MYC-driven TN tumors, we took advantage of recently developed PDX mouse models of breast cancer[19], which have varying expression levels of MYC and PIM1 (**Fig. 3h**). The HCI-002 PDX, which was derived from a primary tumor collected before treatment of the patient with systemic chemotherapy, showed a poorly differentiated TN phenotype (**Supplementary Table 2**)[19] and had the highest level of MYC expression of the three PDX models tested in this study (**Fig. 3h**). PDX tumors were orthotopically transplanted into the mammary gland of immunocompromised mice and were allowed to grow to a volume of 400–450 mm^3 before treatment was initiated with 75 mg/kg SGI-1776, 100 mg/kg NVP-LGB321 (a structurally distinct, newer generation pan–PIM kinase inhibitor from Novartis)[20] or vehicle control daily via oral gavage for 14 d. PIM447 (a compound structurally similar to NVP-LGB321; Novartis)[21] is currently being evaluated in multiple phase 1 and 2 trials for treatment of hematopoietic cancers. Vehicle-treated HCI-002 tumors rapidly reached the ethical end point of this study (**Fig. 3i–k**). In contrast, SGI-1776 treatment markedly decreased tumor growth, whereas NVP-LGB321 treatment induced partial tumor regression (**Fig. 3j,k**). PIM-inhibitor-treated tumors showed a significant decrease in the number of the proliferating (Ki67$^+$) cells (**Fig. 3l**) and a modest increase in the number of apoptotic cells (as assessed by TUNEL staining) (**Supplementary Fig. 5**). To confirm that PIM inhibitor sensitivity *in vivo* was dependent on elevated MYC expression, we used two additional PDX tumor lines, HCI-004 and HCI-009. These PDX tumors were orthotopically transplanted into the mammary gland of immunocompromised mice and allowed to grow to a volume of 400–450 mm^3 before treatment was initiated with

Figure 3 TNBC cells with increased MYC expression are sensitive to PIM kinase inhibition *in vitro* and *in vivo*. (**a**) Representative western blot analysis ($n = 3$) of PIM1 and MYC expression in HMECs and a panel of breast cancer cell lines. Actin was used as a loading control. (**b**) Western blot analysis ($n = 3$) for expression of PIM1 in a panel of breast cancer cell lines after treatment with a pool of *PIM1*-specific siRNAs or a nonspecific control (CTL) siRNA for 60 h. Actin was used as a loading control. (**c–f**) The effects of *PIM1* knockdown in HMECs and a panel of breast cancer cell lines on cell proliferation, as assessed by cell counts (**c**), and apoptosis, as assessed by annexin V and 7-aminoactinomycin D (7-AAD) staining (**e**). Also shown are correlations between levels of MYC (left) or PIM1 (right) and either sensitivity to inhibition of cell proliferation (**d**) or induction of cell death (**f**), as determined by Pearson correlation. In **d,f**, each dot indicates a cell line, and the relative sensitivity of each cell line (*y* axis) refers to the ratio of the mean value of *PIM1*-specific siRNA-treated samples relative to the mean value of control-siRNA-treated samples. The experiments in **c,e** were independently repeated three times in triplicate. Error bars represent means ± s.e.m. *P* values were calculated by two-tailed *t*-test comparing the control-siRNA-treated group to each of the experimental groups. *P < 0.05, **P < 0.01, ***P < 0.001; n.s., not significant. (**g**) *In vivo* growth of MDA-MB-231 (top) and T47D (bottom) xenograft tumors in nude mice that were treated with or without (control; treatment with diluent only) the small-molecule PIM kinase inhibitor SGI-1776 (at 75 mg/kg via oral gavage, daily, for 2 weeks; MDA-MB-231, $n = 6$ mice per treatment group; T47D, $n = 5$ mice per treatment group). The percentage change in tumor volume was calculated for each animal. Error bars represent means ± s.e.m. *P* values were calculated by two-tailed *t*-test comparing the control-treated group to the SGI-1776-treated group. (**h**) Representative western blot analysis ($n = 3$) of PIM1 and MYC expression in a panel of previously reported patient-derived orthotopic breast tumor xenografts. PIM1 and MYC levels in nontumorigenic breast tissue were assessed in breast organoids derived from tissue collected through breast reduction mammoplasty. Numbers shown indicate the relative protein expression of MYC in these PDX tumors. Actin was used as a loading control. (**i**) Representative micrographs ($n = 3$ mice in each treatment group) of HCI-002 PDX tumors before (day 0) and after 2 weeks of treatment with SGI-1776 (75 mg/kg), or after control treatment with diluent (oral gavage, daily, for two weeks). Tumor chunks, approximately at 4~6 mm^3 in volume, were orthotopically transplanted into the cleared mammary fat pads of female NOD–SCID mice and allowed to reach ~450 mm^3 in volume before treatment was initiated. Red arrowheads indicate tumors. (**j,k**) The effects of PIM kinase inhibitors SGI-1776 ($n = 6$ mice in each treatment group) (**j**) and NVP-LGB321 ($n = 7$ mice in each treatment group) (**k**) on ethical end-point survival (left) and *in vivo* growth (right). Ethical end-point survival shows the fraction of surviving mice as mice were removed from the experiment after the size of their tumor reached the institutional limit of reaching or exceeding 2 cm in any one dimension. The percentage change in tumor volume was calculated for each animal. Error bars represent means ± s.e.m. *P* values were calculated by two-tailed *t*-test unless otherwise indicated.
(**l**) Representative micrographs (left) and quantification (right) of Ki67 staining in PDX tumors *in vivo*, collected 24 h after the final treatment of the mice with the indicated PIM inhibitor or with control diluent ($n = 3$ mice in each treatment group). Scale bars, 100 μm. Error bars represent means ± s.e.m. *P* values were calculated by two-tailed *t*-test. (**m,n**) Relative tumor volume of orthotopic HCI-004 (**m**) or HCI-009 (**n**) tumor xenografts in NOD–SCID mice that were treated with vehicle ($n = 5$ mice per group) or 100 mg/kg NVP-LGB321 ($n = 3$ mice per group) daily for 2 weeks. The percentage change in tumor volume was calculated for each animal. Error bars represent means ± s.e.m. *P* values were calculated by two-tailed *t*-test comparing the control-treated group to the NVP-LGB321-treated group. (**o**) Relative tumor volume of orthotopic TetO-MMTV;TRE-*MYC* allografts in FVB/N mice over time. Immediately following orthotopic transplant, mice were maintained on doxycycline, and after the tumors reached 1 cm in any dimension, the mice were treated with either vehicle ($n = 5$) or NVP-LGB321 ($n = 5$) (100 mg/kg, daily for 12 d), or they were taken off doxycycline at day 7 ($n = 5$). The percentage change in tumor volume was calculated for each animal. Error bars represent means ± s.e.m. *P* values were calculated by two-tailed *t*-test comparing the control-treated group to the NVP-LGB321-treated group.

100 mg/kg NVP-LGB321 or vehicle control daily via oral gavage for 14 d. NVP-LGB321 treatment of HCI-004 tumors, which showed an intermediate level of elevated MYC expression (**Fig. 3h**), significantly attenuated tumor growth, but tumor growth was not completely inhibited (**Fig. 3m**). The marked effect of drug treatment on the growth HCI-004 tumors that was observed

during the course of treatment was maintained even after treatment was discontinued (**Supplementary Fig. 6**). In contrast, HCI-009 tumors, which showed a low level of MYC expression similar to that found in nontumor mammary tissue (**Fig. 3h**), did not show significant sensitivity to NVP-LGB321 during the course of treatment (**Fig. 3n**).
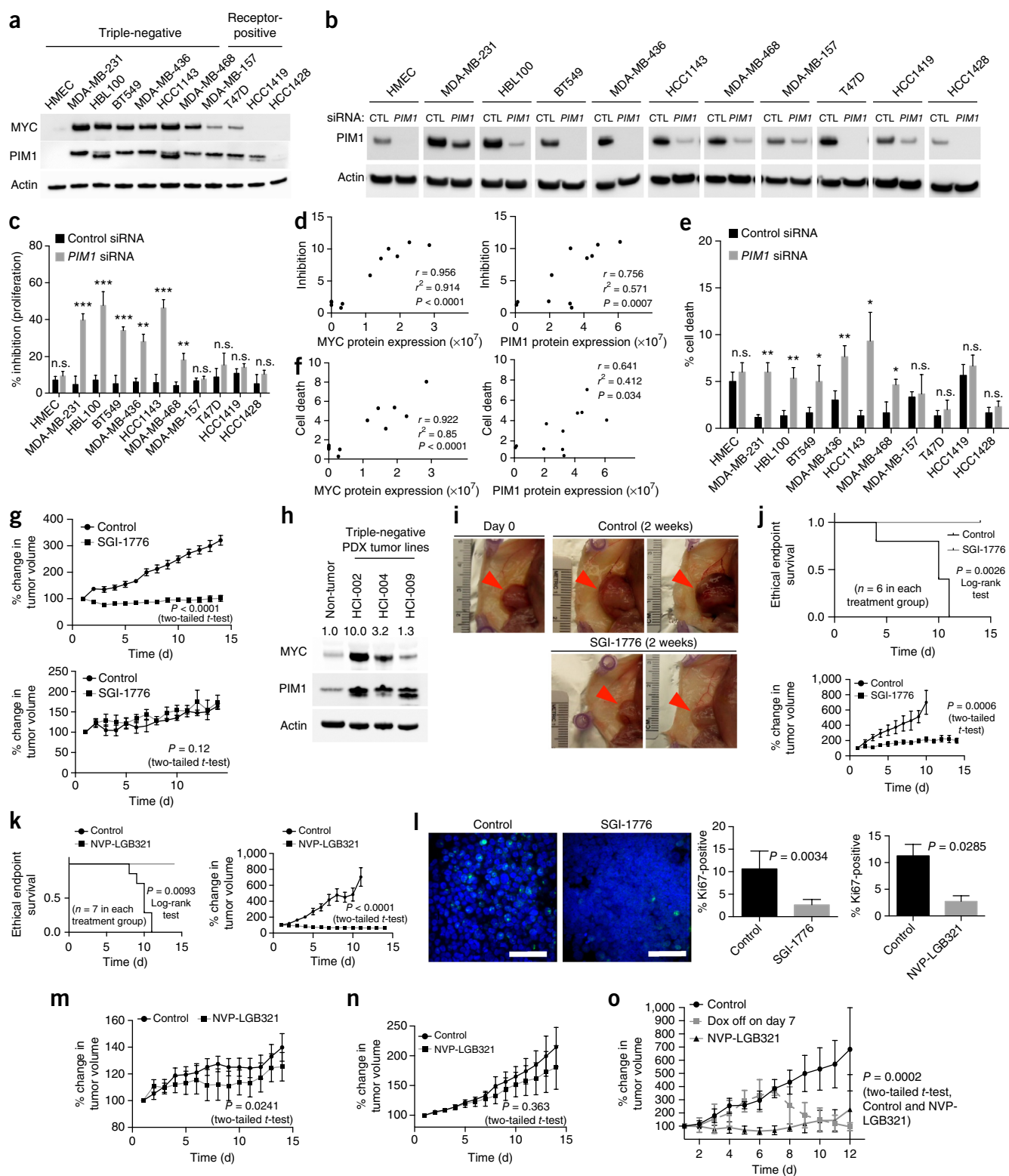
To confirm the finding that TN tumors with increased MYC expression are sensitive to PIM kinase inhibition, we examined the effects of PIM inhibition in a conditional transgenic mouse model of *MYC*-driven breast cancer (TetO-MMTV;TRE-*MYC*)[22]. In this model, tumor growth is dependent on doxycycline-induced MYC expression in mammary tissues, such that removal of doxycycline results in tumor regression (**Fig. 3o**). TetO-MMTV;TRE-*MYC* tumors were orthotopically transplanted into the mammary gland of isogenic mice and allowed to grow to a volume of 400–500 mm[3] before treatment was initiated with 100 mg/kg NVP-LGB321 or vehicle control daily via oral gavage for 12 d. NVP-LGB321 treatment nearly abolished the ability of MMTV-*MYC* allograft tumors to grow (**Fig. 3o**), as compared to control-treated tumor-bearing mice. These data provide genetic evidence that *MYC*-driven breast tumors require PIM kinase activity to maintain tumorigenesis.

To understand the mechanisms by which PIM inhibition abrogates the growth of *MYC*-overexpressing tumors *in vivo*, we examined whether PIM kinase targets are affected in HCI-002 tumors after the tumor-bearing mice were treated with the inhibitors. PIM kinases are known for their role in phosphorylating a number of target proteins, including MYC on Ser62 (which increases MYC transcriptional activity and its oncogenic potential[23,24]), the endogenous cyclin-dependent kinase (CDK) inhibitors p21 and p27 (which negatively controls their activities[25,26]), the CDK phosphatases Cdc25A and Cdc25C (which results in CDK activation[27,28]), the pro-apoptotic BCL2 family member BAD (which inhibits its function[29]) and 4EBP1, a regulator of cap-dependent protein synthesis (which increases the level of protein synthesis[30]). Among these PIM kinase substrates, we found that protein expression and/or phosphorylation status of MYC, p27 and BAD were most consistently and markedly altered in drug-treated PDX tumors (**Fig. 4a** and **Supplementary Fig. 7**). As compared to tumors from mice that were control-treated, tumors from mice that were treated with either of the PIM inhibitors showed marked reductions in total MYC expression and in the amount of Ser62-phosphorylated (pSer62) MYC (**Fig. 4b**). Two weeks of drug treatment did not consist-ently alter the amount of Thr58 phosphorylation (red arrow, **Fig. 4a**), which negatively affects MYC transcriptional activity[24,31]. Notably, some of the tumors from vehicle-treated mice (i.e., 2-week control tumors) showed a marked decrease in Thr58 hyperphosphorylation during primary tumor progression (**Fig. 4a**). These observations suggest that whereas MYC activity increases in control tumors, PIM inhibition results in an overall decrease in MYC activity. Consistent with this hypothesis, we found that expression of a bona-fide MYC transcriptional microRNA (miRNA) target, miR-18 (ref. 32), was uniformly low in tumors from drug-treated mice as compared to those from vehicle-treated mice (**Supplementary Fig. 8**). A similar trend was observed for other MYC-activated miRNAs, namely miR-19b and miR-20a (**Supplementary Fig. 8**). These results are consistent with the observation that the expression of a number of MYC signature genes is altered following PIM kinase inhibitor treatment in sensitive TNBC cell lines[33].

Consistent with a decrease in tumor cell proliferation, as measured by Ki67 staining (**Fig. 3l**), PDX tumors from drug-treated mice showed significantly increased total p27 expression levels (**Fig. 4a,c,d**), whereas protein expression levels of CDKs, CDC25A, CDC25B and p21 were not altered (**Supplementary Fig. 7**). Regulation of p27 involves multiple steps of phosphorylation. Phosphorylation of p27 on Ser10 is required for its binding to the interphase CDKs that are bound to their respective cyclin partners, resulting in inhibition of CDK activity. Thr187 phosphorylation, which is mediated by CDKs, is required for proteasomal degradation of p27. Thr198 is phosphorylated by AKT and also by PIM, and Thr198 phosphorylation triggers p27 binding to 14-3-3 proteins, resulting in nuclear export of p27. Thus, whereas Ser10 phosphorylation of p27 results in its activation, Thr187 and Thr198 phosphorylation both result in the inhibition of p27 function. In addition, Ser10 phosphorylation is required for subsequent phosphorylation on Thr187 and Thr198 (refs. 26,34,35). In PDX tumors from drug-treated mice, levels of Ser10 phosphorylation mirrored those of total p27 (**Fig. 4a,c**), indicating that inhibition of PIM kinase activity does not interfere with Ser10 phosphorylation.

Figure 4 The growth suppressive effects of PIM inhibition on TN tumors involve both loss of MYC function and gain of p27 function. (**a**) Western blot analysis for expression and phosphorylation status of the indicated PIM1 substrates in HCI-002 PDX tumors harvested before (day 0) and after 2 weeks of treatment with either SGI-1776 (75 mg/kg, daily) or NVP-LGB321 (100 mg/kg, daily), or with their respective diluents as controls. Tumors were harvested 24 h after the final drug treatment. Three tumor samples from three independent mice are shown for each time point and treatment condition. The day 0 samples shown are identical across the two columns; blot exposures were made independently and do not control for inter-blot variation in overall band intensity. The red arrow indicates the Thr58 hyperphosphorylated form of MYC. Actin was used as a loading control. (**b**) Total MYC protein expression (relative to actin levels; top) and levels of phosphorylated MYC at Ser62 (relative to total MYC; bottom) in HCI-002 PDX tumors after PIM inhibitor treatment. Three tumor samples from three independent mice are represented for each treatment group. Error bars represent means ± s.e.m. *P* values were calculated by two-tailed *t*-test. (**c**) Total p27 protein expression (normalized to actin levels; top) and levels of phosphorylated forms of p27 (normalized to total p27; bottom) in HCI-002 PDX tumors after PIM inhibitor treatment. Three tumor samples from three independent mice are represented in each treatment group. Error bars represent means ± s.e.m. *P* values were calculated by two-tailed *t*-test. (**d**) Representative confocal images for staining of nuclei (with DAPI, blue) and p27 (green) in HCI-002 PDX tumors from mice that were treated with diluent (control) or SGI-1776 for 2 weeks (top) and quantification of the effects of SGI-1776 and NVP-LGB321 on p27 nuclear accumulation (bottom) (*n* = 3 mice in each treatment group). The percentage of p27-positive cells per high-power field (40×) is shown. Five high-power fields were assessed from each of the three independent tumor samples per treatment group. Error bars represent means ± s.e.m. *P* values were calculated by two-tailed *t*-test. Scale bar, 100 μm. (**e**) Representative western blot analysis (*n* = 3) for p27 protein expression in HMECs and a panel of breast cancer cell lines. Actin was used as a loading control. (**f**) Representative western blot analysis (*n* = 3) for MYC and p27 protein expression in a panel of breast cancer cell lines at the indicated times after treatment with DMSO, SGI-1776 or NVP-LGB321. The cells were treated with the inhibitors at 10 μM, except for HCC1143 cells, which were treated with SGI-1776 at 5 μM due to an excessive amount of cell death using 10 μM. Actin was used as a loading control. (**g**) Representative immunofluorescence images of p27 nuclear accumulation in a panel of TNBC cell lines and quantification of p27 nuclear accumulation (graph) after treatment with NVP-LGB321 (10 μM) or DMSO for 48 h (*n* = 6 for each experimental condition per cell line). Cells were stained with DAPI (blue) and for p27 (green). The number of nuclear p27+ cells was counted in three high-power fields (20×) per sample/slide. Error bars represent means ± s.e.m. *P* values were calculated by two-tailed *t*-test. Scale bar, 100 μm. (**h**) The effects of *MYC* knockdown and p27 upregulation on the proliferation of a panel of TNBC cell lines. The indicated TN lines containing a tetracycline-regulated *CDKN1B* transgene (Tet-p27) were transfected with either a non-targeting control (CTL) or a *MYC*-specific siRNA and cultured for 24 h, and they were then treated with doxycycline (Dox) or control diluent for 48 h. Top, cell numbers relative to the CTL, –Dox group (*n* =3); bottom, MYC and p27 protein levels, with actin used as a loading control. Error bars represent means ± s.e.m. *P* values were calculated by Tukey's multiple comparison test. Actin was used as a loading control. (**i**) Schematic representation of the proposed mechanisms of PIM inhibitor action in MYC-driven TN tumors.

In contrast, the patterns of Thr187 and Thr198 phosphorylation did not follow that of total p27 (**Fig. 4a,c**), as the amount of Thr187- or Thr198-phosphorylated p27 in tumors from drug-treated mice was similar to that observed in tumors from vehicle-treated mice and from mice before drug treatment (day 0 tumors). These observations suggest that in tumors from drug-treated mice, a large pool of CDK-bound, Thr187- and Thr198-unphosphorylated p27 molecules may be

trapped in the nucleus, which interferes with the CDK–p27 recycling mechanism that is essential for cell proliferation. Indeed, co-immunostaining for DAPI and p27 revealed significant nuclear accumulation of p27 in PDX tumors from drug-treated mice (**Fig. 4d**).

The pro-apoptotic BCL2-family member BAD becomes activated after dephosphorylation at conserved sites including Ser112, which in turn results in activation of BAX and BAK, mediators of
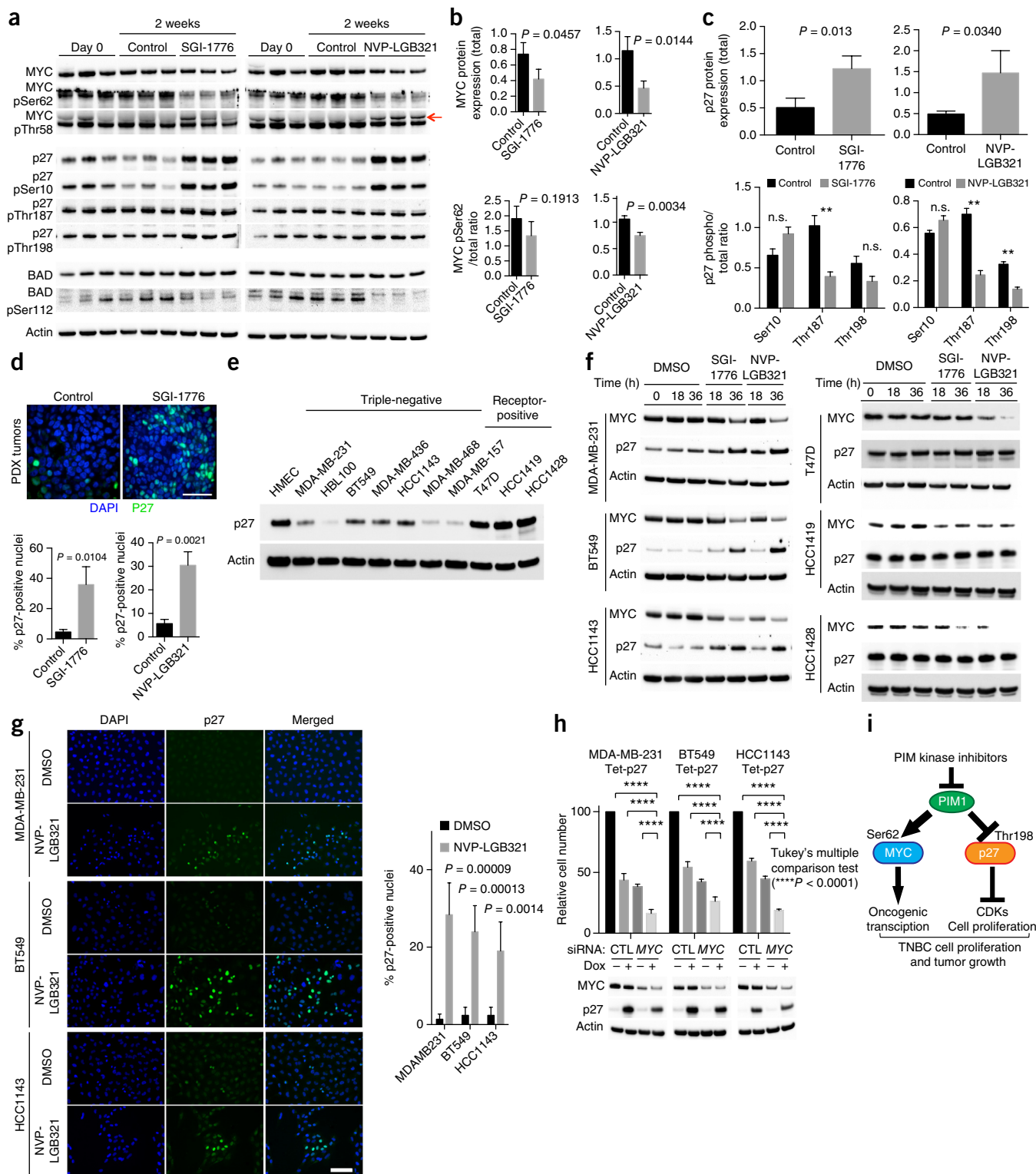
mitochondria-dependent apoptotic cell death, leading to induction of apoptosis[29,36]. Treatment of tumors with either of the PIM inhibitors resulted in a decreased level of Ser112 phosphorylation, with NVP-LGB321 having a greater effect than SGI-1776. (**Fig. 4a**). This effect on BAD phosphorylation may, in part, account for the observation that HCI-002 tumors treated with NVP-LGB231 show partial tumor regression and an increase in the number of apoptotic cells (**Fig. 3k** and **Supplementary Fig. 5**).

We next asked whether the effects observed on MYC and p27 expression after treatment of PDX tumors with PIM inhibitors are also evident in tumor cell lines treated *in vitro*, by using a panel of breast cancer cell lines that show differential sensitivity to PIM inhibitors (**Supplementary Fig. 9**) and have varying endogenous protein expression levels of PIM1 (**Fig. 3a**), MYC (**Fig. 3a**) and p27 (**Fig. 4e**). In the absence of drug treatment, p27 protein expression was markedly lower in TN cell lines than in a nontumor cell line (HMEC) or in RP cell lines. (**Fig. 4e**). Lower *CDKN1B* mRNA levels were also observed in TNBC samples than in HR-positive tumors from clinical data sets (**Supplementary Fig. 10**). PIM inhibitor treatment reduced MYC protein expression in the panel of cell lines examined (**Fig. 4f**), and this effect seemed to be independent of their receptor status or their dependence on MYC for cell proliferation (**Supplementary Fig. 11a–c**). PIM inhibition, however, did not substantially reduce *MYC* mRNA expression (**Supplementary Fig. 12**), suggesting that the reduction in MYC protein expression induced by PIM inhibition probably occurs via post-transcriptional mechanisms. In contrast, PIM inhibitor treatment upregulated p27 expression in TN cell lines that are dependent on MYC for cell proliferation (**Supplementary Fig. 11a–c**) but not in RP cell lines (**Fig. 4f,g**). Similar effects on MYC expression were observed with *PIM1* knockdown using a *PIM1*-specific siRNA (**Supplementary Figs. 11a and 13**). Notably, the sensitivity of the panel of breast cancer cell lines to PIM1 inhibition was more strongly correlated with protein expression levels of MYC and PIM1 (positive correlation) than with baseline p27 protein expression (negative correlation) (**Fig. 3c–f** and **Supplementary Fig. 14**). Finally, TN cell lines that are sensitive to PIM inhibitors showed an induction of nuclear p27 accumulation (**Fig. 4g**), which was also seen *in vivo* after PIM inhibitor treatment of mice with PDX tumors (**Fig. 4d**).

To test whether increased p27 expression alone is sufficient to inhibit TN cell proliferation, we studied the sensitivity of TN lines to increased p27 expression. We conditionally increased p27 expression in the presence or absence of siRNA-mediated *MYC* knockdown using a doxy-cycline-regulated approach (**Fig. 4h**). In doing so, we attempted to achieve an extent of p27 upregulation similar to that observed in PIM-inhibitor-treated PDX tumors *in vivo* (**Fig. 4a**). Induction of p27 over-expression significantly diminished cell proliferation in all of the lines tested (**Fig. 4h**), and induction of p27 overexpression together with *MYC* knockdown resulted in further growth inhibition (**Fig. 4h**). Thus, the near-complete growth inhibition seen in PIM-inhibitor-treated PDX tumors is probably due to cumulative antiproliferative effects of diminished MYC activity and elevated p27 expression (**Fig. 4i**).

Our observation that PIM inhibition results in diminished MYC activity in TN tumors, combined with the previous observation that PIM kinases are non-essential in mice[11], makes PIM an attractive therapeutic target for breast cancer. Moreover, previous observations in numerous breast cancer clinical cohorts have associated diminished p27 expression with poor prognosis[37], and we found that PIM inhibition results in increased levels of nuclear p27. A report by the Cancer Genome Atlas (TCGA) Breast Group indicates that the *CDKN1B* gene, which encodes p27, is neither deleted nor mutated in the vast majority of TN tumor samples[38], supporting the potential use of PIM inhibition in restoring p27 expression and function in these aggressive tumors. In conclusion, our work identifies PIM1 kinase as a factor that is specifically upregulated in TNBC and is a potentially druggable target in tumors that show increased MYC expression.

METHODS

Methods and any associated references are available in the online version of the paper.

Note: Any Supplementary Information and Source Data files are available in the online version of the paper.

1. Foulkes, W.D., Smith, I.E. & Reis-Filho, J.S. Triple-negative breast cancer. *N. Engl. J. Med.* **363**, 1938–1948 (2010).
2. Horiuchi, D. *et al.* MYC pathway activation in triple-negative breast cancer is synthetic lethal with CDK inhibition. *J. Exp. Med.* **209**, 679–696 (2012).
3. Prochownik, E.V. & Vogt, P.K. Therapeutic targeting of Myc. *Genes Cancer* **1**, 650–659 (2010).
4. Kaelin, W.G. Jr. The concept of synthetic lethality in the context of anticancer therapy. *Nat. Rev. Cancer* **5**, 689–698 (2005).
5. Mukhopadhyay, R. *et al.* Promotion of variant human mammary epithelial cell outgrowth by ionizing radiation: an agent-based model supported by *in vitro* studies. *Breast Cancer Res.* **12**, R11 (2010).
6. Littlewood, T.D., Hancock, D.C., Danielian, P.S., Parker, M.G. & Evan, G.I. A modified estrogen receptor ligand-binding domain as an improved switch for the regulation of heterologous proteins. *Nucleic Acids Res.* **23**, 1686–1690 (1995).
7. Kessler, J.D. *et al.* A SUMOylation-dependent transcriptional subprogram is required for Myc-driven tumorigenesis. *Science* **335**, 348–353 (2012).
8. Sato, M. *et al.* MYC is a critical target of FBXW7. *Oncotarget* **6**, 3292–3305 (2015).
9. Bazarov, A.V. *et al.* Telomerase activation by c-MYC in human mammary epithelial cells requires additional genomic changes. *Cell Cycle* **8**, 3373–3378 (2009).
10. Nawijn, M.C., Alendar, A. & Berns, A. For better or for worse: the role of *Pim* oncogenes in tumorigenesis. *Nat. Rev. Cancer* **11**, 23–34 (2011).
11. Mikkers, H. *et al.* Mice deficient for all PIM kinases display reduced body size and impaired responses to hematopoietic growth factors. *Mol. Cell. Biol.* **24**, 6104–6115 (2004).

12. van Lohuizen, M. *et al.* Predisposition to lymphomagenesis in *Pim1* transgenic mice: cooperation with c-Myc and N-Myc in murine leukemia virus–induced tumors. *Cell* **56**, 673–682 (1989).

13. Wang, J. *et al.* Pim1 kinase synergizes with c-MYC to induce advanced prostate carcinoma. *Oncogene* **29**, 2477–2487 (2010).

14. Wang, J. *et al.* Pim1 kinase is required to maintain tumorigenicity in MYC-expressing prostate cancer cells. *Oncogene* **31**, 1794–1803 (2012).

15. Kirschner, A.N. *et al.* PIM kinase inhibitor AZD1208 for treatment of *MYC*-driven prostate cancer. *J. Natl. Cancer Inst.* **107**, dju407 (2014).

16. Xie, Y. *et al.* The 44-kDa Pim-1 kinase directly interacts with tyrosine kinase ETK (BMX) and protects human prostate cancer cells from apoptosis induced by chemotherapeutic drugs. *Oncogene* **25**, 70–78 (2006).

17. Malinen, M. *et al.* Proto-oncogene *PIM1* is a novel estrogen receptor target associating with high-grade breast tumors. *Mol. Cell. Endocrinol.* **365**, 270–276 (2013).

18. Chen, L.S., Redkar, S., Bearss, D., Wierda, W.G. & Gandhi, V. Pim kinase inhibitor SGI-1776 induces apoptosis in chronic lymphocytic leukemia cells. *Blood* **114**, 4150–4157 (2009).

19. DeRose, Y.S. *et al.* Tumor grafts derived from women with breast cancer authentically reflect tumor pathology, growth, metastasis and disease outcomes. *Nat. Med.* **17**, 1514–1520 (2011).

20. Lu, J. *et al.* Pim2 is required for maintaining multiple myeloma cell growth through modulating TSC2 phosphorylation. *Blood* **122**, 1610–1620 (2013).

21. Burger, M.T. *et al.* Identification of *N*-(4-((1*R*,3*S*,5*S*)-3-amino-5-methylcyclohexyl) pyridin-3-yl)-6-(2,6-difluorophenyl)-5-fluoropicolinamide (PIM447), a potent and selective proviral insertion site of Moloney murine leukemia (PIM) 1, 2 and 3 kinase inhibitor in clinical trials for hematological malignancies. *J. Med. Chem.* **58**, 8373–8386 (2015).

22. D'Cruz, C.M. *et al.* c-MYC induces mammary tumorigenesis by means of a preferred pathway involving spontaneous *Kras2* mutations. *Nat. Med.* **7**, 235–239 (2001).

23. Zhang, Y., Wang, Z., Li, X. & Magnuson, N.S. Pim-kinase-dependent inhibition of c-Myc degradation. *Oncogene* **27**, 4809–4819 (2008).

24. Sears, R.C. The life cycle of c-Myc: from synthesis to degradation. *Cell Cycle* **3**, 1133–1137 (2004).

25. Zhang, Y., Wang, Z. & Magnuson, N.S. Pim-1-kinase-dependent phosphorylation of p21Cip1 (WAF1) regulates its stability and cellular localization in H1299 cells. *Mol. Cancer Res.* **5**, 909–922 (2007).

26. Morishita, D., Katayama, R., Sekimizu, K., Tsuruo, T. & Fujita, N. Pim kinases promote cell cycle progression by phosphorylating and downregulating *p27Kip1* at the transcriptional and post-transcriptional levels. *Cancer Res.* **68**, 5076–5085 (2008).

27. Bachmann, M. *et al.* The oncogenic serine–threonine kinase Pim-1 directly phosphorylates and activates the G2/M-specific phosphatase Cdc25C. *Int. J. Biochem. Cell Biol.* **38**, 430–443 (2006).

28. Mochizuki, T. *et al.* Physical and functional interactions between Pim-1 kinase and Cdc25A phosphatase. Implications for the Pim-1-mediated activation of the c-Myc signaling pathway. *J. Biol. Chem.* **274**, 18659–18666 (1999).

29. Yan, B. *et al.* The PIM-2 kinase phosphorylates BAD on serine 112 and reverses BAD-induced cell death. *J. Biol. Chem.* **278**, 45358–45367 (2003).

30. Fox, C.J. *et al.* The serine–threonine kinase Pim-2 is a transcriptionally regulated apoptotic inhibitor. *Genes Dev.* **17**, 1841–1854 (2003).

31. Wang, X. *et al.* Phosphorylation regulates c-Myc's oncogenic activity in the mammary gland. *Cancer Res.* **71**, 925–936 (2011).

32. O'Donnell, K.A., Wentzel, E.A., Zeller, K.I., Dang, C.V. & Mendell, J.T. c-Myc-regulated microRNAs modulate *E2F1* expression. *Nature* **435**, 839–843 (2005).

33. Brasó-Maristany, F. *et al.* PIM1 kinase regulates cell death, tumor growth and chemotherapy response in triple-negative breast cancer. *Nat. Med.* **22**, 1303–1313 (2016).

34. Mohanty, A.R. *et al.* Successive phosphorylation of p27KIP1 protein at Ser10 and C terminus crucially controls its potency to inactivate Cdk2. *J. Biol. Chem.* **287**, 21757–21764 (2012).

35. Fujita, N., Sato, S., Katayama, K. & Tsuruo, T. Akt-dependent phosphorylation of p27Kip1 promotes binding to 14-3-3 and cytoplasmic localization. *J. Biol. Chem.* **277**, 28706–28713 (2002).

36. Czabotar, P.E., Lessene, G., Strasser, A. & Adams, J.M. Control of apoptosis by the BCL-2 protein family: implications for physiology and therapy. *Nat. Rev. Mol. Cell Biol.* **15**, 49–63 (2014).

37. Chu, I.M., Hengst, L. & Slingerland, J.M. The Cdk inhibitor p27 in human cancer: prognostic potential and relevance to anticancer therapy. *Nat. Rev. Cancer* **8**, 253–267 (2008).

38. Cancer Genome Atlas Network. Comprehensive molecular portraits of human breast tumors. *Nature* **490**, 61–70 (2012).

ONLINE METHODS

Human mammary epithelial cells expressing the *MYC-ER* transgene. Primary human mammary epithelial cells (HMECs) were derived from histologically normal breast tissues and cultured as previously described[5]. Where indicated, primary mammary organoids were used as a source of nontumor total protein lysates. The derived cells were infected with lentivirus expressing *CDKN2A* (which encodes p16, and which we hereafter refer to as *p16*)-specific shRNA[39] and were further infected with pBabe-*MYC-ER* virus[6]. The resulting cells were named B1389-shp16-*MYC-ER* (referred to as HMEC-*MYC-ER* cells). Expression of the *p16*-specific shRNA delays the onset of senescence in HMEC-*MYC-ER* cells, but the cells are not immortalized and undergo spontaneous senescence as the cells are continuously cultured[40]. HMEC-*MYC-ER* cells were used for the screen within 12 passages of derivation to minimize the accumulation of spontaneous genomic alterations unrelated to MYC activation. HMEC-*MYC-ER* cells were treated with 500 nM 4-hydroxytamoxifen (TAM) to induce MYC activation.

Kinome MYC synthetic lethal shRNA screen. The screen in this study was performed using the Open Biosystems Human GIPZ Lentiviral Human Kinase Library v1 (RHS4808). In this library, approximately 600 kinases are targeted by 2,000 independent shRNA clones; each kinase is targeted by ~7 independent clones. The lentiviral supernatants were produced by the UCSF VIRACORE (http://viracore.ucsf.edu) in a 96-well format by transfecting 293T cells with individual shRNA clones together with packaging plasmids VsVg and Delta 8.9. Approximately 90 µl of unconcentrated viral supernatant was obtained from each well. HMEC-*MYC-ER* cells were seeded onto 96-well plates (2,000 cells/well) and incubated with 40 µl of viral supernatant in the presence of hexadimethrine bromide (polybrene; Sigma) at 7 µg/ml. The cells were incubated with the viruses for 20–21 h, at which time the virus-containing medium was replaced by fresh medium without or with TAM. After 48 h of incubation without or with TAM, the cells were subjected to CellTiter96 Aqueous One-Solution Cell Proliferation assay (Promega) to determine cell proliferation from the time of MYC activation. The percentage of cell death was calculated by subtracting the values obtained before MYC activation from the final values, and the percentage decrease in proliferation was determined by subtracting the final values in the +TAM plates from those in the −TAM plates. Candidate synthetic lethal genes targeted by the shRNA clones that induced cell death in HMECs irrespective of MYC activation status were not pursued further.

Bioinformatic analyses. Four different clinical data sets were used for bioinformatics analyses. The TCGA breast invasive carcinoma data set was sourced from data generated by TCGA Research Network (http://cancergenome.nih.gov/; made available on the University of California, Santa Cruz (UCSC) Cancer Browser). The chemotherapy-naive data set[41] was obtained from the UCSC Cancer Browser. Series matrix files for I-SPY1 (accession: GSE22226)[42] and the pooled neoadjuvant chemotherapy-treated cohort (accession: GSE25066)[43] were downloaded from Gene Expression Omnibus (GEO) and extracted into a usable format with the GEOquery R package[44]. Multiple probes corresponding to the same gene were collapsed using the 'MaxMean' method in the weighted gene correlation network analysis (WGCNA) R package[45,46].

To generate bar plots, each of the data sets was stratified into three groups based on receptor status: samples that were positive for the HER2 (ERBB2) receptor tyrosine kinase (HER2+), those that were positive for the estrogen and/or progesterone receptors (HR+), and those that were triple-negative (TN). Log-transformed and median-centered *PIM1* expression values were derived for the respective groups and visualized using the ggplot2 R package[47].

To generate Kaplan–Meier plots, samples negative for both the estrogen and progesterone receptors (HR−) were isolated from each of the data sets and dichotomized by *PIM1* expression at an optimal threshold. This optimal threshold was defined by considering values between the 10th and 90th percentile and selecting the cut point that yielded two groups with the most significant differences in disease-recurrence-free or distant-metastasis-free survival based on the log-rank test (**Fig. 2b**). Kaplan–Meier plots were then generated for the respective groups using the survival R package[48]. In addition to dichotomization at the optimal threshold, we also evaluated association between *PIM1* expression as a continuous variable and survival outcomes using Cox proportional-hazards modeling (**Fig. 2c**).

We next assessed whether *PIM1* expression and the MYC signature score were independently associated with survival outcomes using a multivariate Cox proportional-hazards model that includes both of these factors as continuous explanatory variables (**Fig. 2d**). To generate the MYC signature score, expression data were mapped onto the MYC gene signature score centroid[2] by gene symbol, and the score was computed as the Pearson correlation of each tumor's expression profile to the signature centroid. This survival analysis was repeated specifically for HR-positive and HR-negative subsets of these data sets as well. PR status was not available for the chemotherapy-naive data set; accordingly, ER− and ER+ subsets were considered instead.

Breast cancer cell lines. A panel of established human breast cancer cell lines, including the cell culture conditions, has been previously described[49]. A PCR-based method was routinely used to ensure that all of the cells used in this study were mycoplasma free. The primers initially used are: forward-ACTCCTACGGGAGGCAGCAGT A; reverse-TGCACCATCTGTCACTCTG TTAACCTC. Additionally, the Universal Mycoplasma Detection Kit (ATCC, 30-1012K) was used to ensure that cells were not infected with mycoplasma.

Mouse experiments. All protocols described in this and other sections regarding mouse studies were approved by the UCSF Institutional Animal Care and Use Committee; the ethical end point for mammary tumor transplantation experiments was reached when a tumor reached ≥2 cm in any single dimension. To subcutaneously grow MDA-MB-231 and T47D tumors, the cells (3 × 10^6 for MDA-MB-231, and 1 × 10^7 for T47D) were subcutaneously injected into immunodeficient female mice (BALB/c nude/nude) aged 6~8 weeks. The tumors were allowed to grow to 150~200 mm³ in volume, at which time drug treatment was initiated. The animals were treated with an experimental pan–PIM kinase small-molecule inhibitor SGI-1776 (purchased from Selleckchem, S2198), dissolved in 5% dextrose/water solution, at 75 mg/kg, or vehicle alone, daily, via oral gavage. SGI-1776 at 75 mg/kg was previously shown to be effective in causing regression of xenografted acute myeloid leukemia cells in mice[50].

PDX tumors were grown as previously described[19]. For PIM inhibitor treatment, PDX tumor chunks were transplanted into cleared mammary fad pads of NOD–SCID immune-deficient female mice aged 4.0~4.5 weeks, and the grafted tumors were allowed to reach ~450 mm³ in volume, at which time drug treatment was initiated. The mice were treated with either SGI-1776 at 75 mg/kg or with a newer-generation PIM kinase inhibitor NVP-LGB321 (refs. 20,51), which is under clinical development and was provided by Novartis, or with the respective vehicle alone. The NVP-LGB321 solution was prepared in 50 mM sodium acetate buffer (pH 4.6) and was administered at 100 mg/kg, daily, via oral gavage. For the HCI-004 study, some of the mice were monitored for an additional 36 d after 2 weeks of drug treatment was completed.

TetO-MMTV;TRE-*MYC* mice were generated as previously described[22]. Mice were bred and maintained off of doxycycline. At 12–15 weeks of age, female mice were put on doxycycline (200 mg/kg doxy chow, Bio-Serv) to induce MYC expression and tumorigenesis. Mice were euthanized as per ethical guidelines (tumors reaching 2 cm in any single dimension), and the harvested tumors were flash-frozen in liquid nitrogen. To perform orthotopic allograft studies, flash-frozen MMTV-*MYC* tumors were thawed, cut into smaller chunks and transplanted into cleared mammary fat pads of 4-week-old wild-type female FVB/N mice. Tumor-bearing FVB/N mice were treated with NVP-LGB321 as described for the PDX tumor-bearing NOD–SCID mice.

Western blot analyses. Tumors or cell lysates were prepared as previously described[2]. The primary antibodies used in this study were to the following proteins: β-actin (clone AC-15, Sigma A1978, 1:10,000), BAD (clone Y208, Abcam, ab32445, 1:1,000), BAD(pSer112) (clone EPR1891(2), Abcam, ab129192, 1:750), Cdc25A (Sigma, HPA005855, 1:250), Cdc25C (clone 5H9, Cell Signaling, 4688, 1:500), CDK1 (clone 17, Santa Cruz Biotech., sc-54, 1:200), CDK2 (clone D-12, Santa Cruz Biotech., sc-6248, 1:200), CDK4 (clone C-22, Santa Cruz Biotech., sc-260, 1:200), 4EBP1 (clone 53H11, Cell Signaling, 9644, 1:750), 4EBP1(pThr37,Thr46) (clone 236B4, Cell Signaling, 2855, 1:750), 4EBP1(pSer65) (Cell Signaling, 9451, 1:1,000), c-MYC (clone Y69, Epitomics, 1472-1, 1:10,000), c-MYC(pThr58) (Applied Biological Materials, Y011034, 1:500), c-MYC(pSer62)

(clone 33A12E10, Abcam, ab78318, 1:1,000), p21 (BD Pharmingen, 556430, 1:500), p27 (BD Transduction Lab., 610241, 1:1,000), p27(pSer10) (clone EP233(2)Y, Abcam, ab62364, 1:10,000), p27(pThr187) (Abcam, ab75908, 1:500), p27(pThr198) (R&D Systems, AF3994, 1:200), PIM1 (clone EP2645Y, Abcam, ab75776, 1:2,000, and GeneTex, GTX61985, 1:2,000), PIM2 (clone EPR6987, Abcam, ab129057, 1:1,000, and clone D1D2, Cell Signaling, 4730, 1:1,000). The secondary antibodies used were goat anti-mouse-IgG–HRP (Santa Cruz Biotech., sc-2055, 1:10,000) and goat anti-rabbit-IgG–HRP (Santa Cruz Biotech., sc-2054, 1:10,000). The ECL reaction was done using the Bio-Rad Clarity Western ECL Substrate, and chemiluminescent signals were acquired with the Bio-Rad ChemiDoc XRS+ System or the Bio-Rad ChemiDoc Touch Imaging system equipped with a supersensitive CCD camera. Where indicated, unsaturated band intensities were quantified using Bio-Rad Image Lab software. Actin was primarily used as the loading control; however, Bio-Rad TGX Stain-Free protein gels, which fluorescently label all the tryptophan residues of proteins in gels, were also used for normalization of western blot bands. Uncropped blots for western blot analyses are in **Supplementary Figures 15–21**.

Indirect immunofluorescence microscopy. For immunostaining of primary PDX tissues for Ki67 and p27 protein expression, paraffin-embedded tissue samples were sectioned, deparaffinized and rehydrated. Antigen retrieval was done using 10 mM sodium citrate, pH 6.0. Nonspecific binding sites were blocked with 5% normal goat serum. The blocked samples were incubated with primary antibodies against Ki67 (Abcam, ab833, 1:400) and p27 (BD Transduction Laboratories, 610241, 1:500) overnight at 4 °C. After washing, the samples were incubated for 1 h at room temperature with the fluorescently labeled secondary antibodies Alexa-Fluor-488-conjugated goat anti-mouse-IgG (Invitrogen, A-11001, 1:500) or Alexa-Fluor-488-conjugated goat anti-rabbit-IgG (Invitrogen, A-11008, 1:500), respectively. The samples were then embedded in mounting medium containing DAPI (Dako), and the images were acquired using the Zeiss Axiovert 200M spinning disk confocal system equipped with Micro Manager software. The acquired images were processed using ImageJ (Fiji). To quantify the percentage of Ki67- and p27-positive cells per high-power field (40×), at least five images per sample were taken for each of three drug-treated and three control-treated samples. For each image, we determined the number of DAPI-positive nuclei using ImageJ, and the number of Ki67- or p27-positive cells was counted manually.

For immunostaining of the established breast cancer cell lines for p27 protein expression, the cells were fixed with 4% paraformaldehyde in 6-well plates, blocked with 3% normal goat serum and treated with the p27-specific primary antibody (BD Transduction Lab., 610241, 1:500) and with secondary antibody (Alexa-Fluor-488-conjugated goat anti-mouse-IgG, Invitrogen, A-11029, 1:500). Nuclear staining was done through the use of the mountant ProLong Gold anti-fade reagent with DAPI (Life Technologies). The images were acquired using the Zeiss Axioplan 2 epifluorescence imaging system equipped with the Micro Manager software.

Real-time quantitative PCR. Total RNA from the PDX tumor samples was extracted using the mirVana miRNA isolation kit (Ambion) according to the manufacturer's instructions. Real-time PCR was carried out using TaqMan probes (Applied Biosystems) specific for miR-18a, miR-19b and miR-20a, and the values were normalized relative to the expression of the small nucleolar RNA, C/D box 48 (*SNORD48*; also known as *RNU48*) endogenous control gene.

siRNA experiments. Gene-specific pools of siRNAs were purchased from GE Dharmacon (siGENOME SMARTpool siRNA, M-003923-00-0005 for the *PIM1*-specific pool, M-005359-00-0005 for the *PIM2*-specific pool and M-005359-00-0005 for the *MYC*-specific pool), and siRNA transfection was performed using Lipofectamine RNAiMAX Transfection Reagent (Life Technologies) via the reverse-transfection method, as previously described[2]. To sufficiently reduce PIM1 protein expression, particularly in the panel of triple-negative breast cancer cell lines, it was necessary to use the *PIM1*-spcific siRNA at the highest suggested dose (120–150 pmol per well in 6-well cell culture dishes). Even at these concentrations, we observed that some of the cell lines started to recover endogenous levels of *PIM1* expression in less than 60 h post siRNA reverse-transfection (for example, MDA-MB-231 cells in **Fig. 3b** and **Supplementary**

Fig. 4a). *PIM2*-specific siRNA was used at 120 pmol per well in 6-well cell culture dishes. To knock down *MYC* expression in breast cancer cell lines, the *MYC*-spcific siRNA was used at 60 pmol per well in 6-well cell culture dishes. For control siRNAs, we used both Dharmacon siGENOME GAPD Control siRNA (D-001140-01-05) and siGENOME RISC-Free siRNA (D-001220-01-05); these two siRNAs caused similar and acceptable levels of cytotoxicity.

In vitro cell proliferation and cell death assays. Unless otherwise noted, cell proliferation and cell death were assessed by performing a flow-cytometry-based Guava ViaCount viability assay (Millipore). For the experiments shown in **Figure 3e**, Guava Nexin reagent (Millipore) was used to specifically determine the number of apoptotic and dead cells that were positive for annexin V and/or 7-AAD staining. For the experiments shown in **Figure 4i**, cell number was determined by counting the cells using the Countess Automated Cell Counter (Life Technologies) according to the manufacturer's instructions.

Transgenic breast cancer cell lines. A doxycycline (tet)-regulated *CDKN1B* expression construct was generated by subcloning a full-length human *CDKN1B* cDNA (with a GCCACC Kozak sequence in front of the start codon) into the BamH1–EcoR1 sites of the multiple cloning site of pLVX-Tight-Puro lentiviral expression plasmid (Clontech). To produce recombinant lentiviral supernatants, 293FT cells were cotransfected with the ViraPower Lentiviral Packaging Mix (Life Technologies) and either pLVX-Tight-Puro-p27 or the transactivator construct pLVX-Tet-ON Advanced, using the Lipofectamine 2000 Transfection Reagent. Breast cancer cell lines were co-incubated with the resulting Tight-Puro-p27 supernatant and the Tet-ON Advanced supernatant, mixed at the ratio of 3:1, in the presence of polybrene at 6 µg/ml for 24 h. We found that the degree to which doxycycline (100 ng/ml) induced an increase in p27 protein expression was similar to the degree of p27 upregulation in PIM-inhibitor-treated PDX tumor tissues (for example, **Fig. 4a,h**). Thus, for the experiments shown in **Figure 4i**, p27 upregulation was achieved by treating the established transgenic cell lines with doxycycline at 100 ng/ml.

TUNEL staining. TUNEL staining was carried out on PDX tumor sections using the ApopTag Peroxidase *In situ* Apoptosis Detection Kit (Millipore), according to the manufacturer's instructions.

Statistical analyses. All results are shown as mean ± s.e.m., unless otherwise indicated. Statistical analyses (two-tailed *t*-test, Pearson correlation, log-rank test and Tukey's multiple-comparison test) were performed using Prism 6 (version 6.0f) from GraphPad Software, Inc. and R (Version 3.1.0), taking into consideration the assumptions required for the respective tests. $P < 0.05$ was considered to indicate statistical significance throughout the study. All cell-based *in vitro* experiments were independently repeated three times in triplicate. No statistical method was used to pre-determine sample size throughout this study. For animal experiments, efforts were made to achieve the scientific goals of this study with the minimum number of animals. With respect to randomization, for animal experiments, tumor-bearing mice of similar tumor burden were equally divided into the control and experimental groups for subsequent drug treatment. For immunostaining (DAPI and p27) and TUNEL staining of PDX tumor samples, the scoring process was carried out in a blinded fashion. No experimental samples were excluded throughout this study, with the exception that animals that experienced unexpected, acute illness and/or injury were removed per the veterinarian's order.

Code availability. All custom computer code and data sets used for bioinformatics analyses, as outlined below, are freely available for download and/or use on Github at https://github.com/snjvb/pim_kinase. The raw data and processing routines are included for the following data sets (directory names for the respective data sets are indicated in parentheses): TCGA breast invasive carcinoma data set (TCGA_BRCA_exp_HiSeqV2-2014-08-28), chemotherapy-naive data set (YauGeneExp-2011-11-11), I-SPY1 data set (ispy1_082814) and pooled neoadjuvant-chemotherapy-treated data set (gse25066_091114). The core analysis pipeline, written in the R programming language, is included in the file 'pim_analysis.r'. Additional code for multivariate analysis of MYC signature and *PIM1* expression are available upon request.

39. Narita, M. *et al.* Rb-mediated heterochromatin formation and silencing of E2F target genes during cellular senescence. *Cell* **113**, 703–716 (2003).

40. Bazarov, A.V. *et al.* p16INK4a-mediated suppression of telomerase in normal and malignant human breast cells. *Aging Cell* **9**, 736–746 (2010).

41. Yau, C. *et al.* A multigene predictor of metastatic outcome in early-stage hormone-receptor-negative and triple-negative breast cancer. *Breast Cancer Res.* **12**, R85 (2010).

42. Esserman, L.J. *et al.* Chemotherapy response and recurrence-free survival in neoadjuvant breast cancer depends on biomarker profiles: results from the I-SPY 1 TRIAL (CALGB 150007/150012; ACRIN 6657). *Breast Cancer Res. Treat.* **132**, 1049–1062 (2012).

43. Hatzis, C. *et al.* A genomic predictor of response and survival following taxane-anthracycline chemotherapy for invasive breast cancer. *J. Am. Med. Assoc.* **305**, 1873–1881 (2011).

44. Davis, S. & Meltzer, P.S. GEOquery: a bridge between the Gene Expression Omnibus (GEO) and BioConductor. *Bioinformatics* **23**, 1846–1847 (2007).

45. Langfelder, P. & Horvath, S. WGCNA: an R package for weighted correlation network analysis. *BMC Bioinformatics* **9**, 559 (2008).

46. Langfelder, P. & Horvath, S. Fast R functions for robust correlations and hierarchical clustering. *J. Stat. Softw.* **46**, i11 (2012).

47. Wickham, H. *ggplot2* (Springer Science and Business Media, 2009).

48. Therneau, T.M. *Modeling Survival Data: Extending the Cox Model* (Springer Science and Business Media, 2000).

49. Neve, R.M. *et al.* A collection of breast cancer cell lines for the study of functionally distinct cancer subtypes. *Cancer Cell* **10**, 515–527 (2006).

50. Chen, L.S., Redkar, S., Taverna, P., Cortes, J.E. & Gandhi, V. Mechanisms of cytotoxicity to Pim kinase inhibitor, SGI-1776, in acute myeloid leukemia. *Blood* **118**, 693–702 (2011).

51. Garcia, P.D. *et al.* Pan–PIM kinase inhibition provides a novel therapy for treating hematologic cancers. *Clin. Cancer Res.* **20**, 1834–1845 (2014).